CHAPTER II

BACKGROUND

This section serves as a summary of the literature review, focusing on topics relevant to the research. It begins with the classification of electrochemical energy storage sources. The subsequent part delves into lithium-ion batteries, with a particular emphasis on glass batteries, followed by an exploration of their distinctive characteristics. The chapter concludes with a clear elucidation of the covered objectives and the research efforts undertaken within the scope of this academic thesis. sources

2.1 Classification of electrochemical energy storage

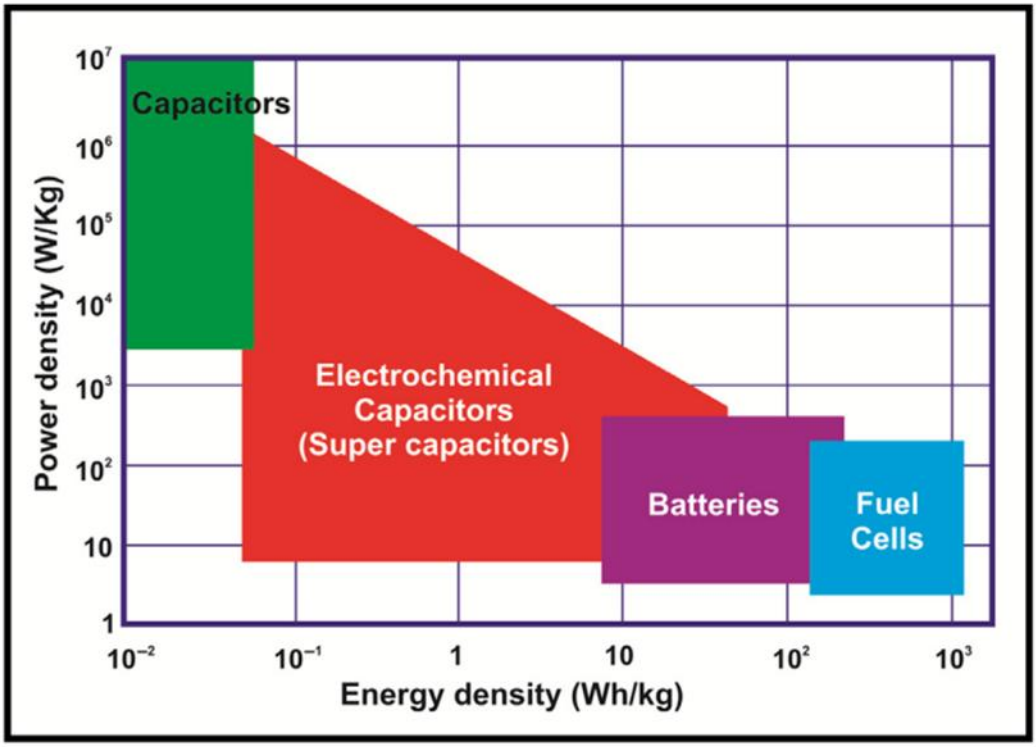

Figure 2.1 Ragone plot of various energy storage devices power and energy density (Sagadevan et al., 2021).

Energy storage devices (ESD) is characterized by their energy and power density. The Ragone plot, depicted in Figure 2.1, has long served as a standard reference in the battery research community (Christen and Carlen, 2000). Electrochemical Energy Storage (EES) is widely utilized for power generation and is now an integral part of portable electronics. It also finds applications in electrifying the transportation sector through batteries. The classification of ESS can be categorized as follows.

2.1.1 Fuel cells (FCs)

Fuel cells are energy conversion devices that directly convert the chemical energy from various fuels, into electrical energy with significantly higher efficiency compared to conventional power generation sources, both theoretically and in practice (Abdelkareem et al., 2021). Fuel cells have high energy density content but exhibit low power density due to their slower kinetic reactions (Sagadevan et al., 2021).

2.1.2 Batteries

Batteries are critical components in modern technology, enabling the seamless operation of electronic devices, from smartphones to electric vehicles. Their development has advanced significantly, with innovations focusing on higher energy density, and enhanced safety. In addition to their technological benefits, batteries contribute to reducing carbon emissions by supporting the integration of renewable energy systems like solar and wind power. As research continues, next-generation batteries are expected to become more efficient, cost-effective, and sustainable, further revolutionizing energy storage solutions. (Weber et al., 2011).

2.1.3 Supercapacitors

Supercapacitors are unique energy storage devices characterized by their electrostatic charge separation mechanism, setting them apart from traditional capacitors and batteries. They excel in delivering rapid bursts of power, boasting durability and high efficiency in charge-discharge cycles. However, supercapacitors are sensitive to temperature fluctuations, which can adversely affect their performance and lifespan. Additionally, their lower energy density compared to batteries makes them less suitable for long-term energy storage applications without frequent recharging (González, Goikolea, Barrena, and Mysyk, 2016; Hannan, Hoque, Mohamed, and Ayob, 2017; Sagadevan et al., 2021).

2.1.4 Capacitors

Capacitors store electrical energy at the interface between an electrolyte and a solid electrode. Capacitors have the highest power density because of their rapid charge and discharge capabilities, but they store the lowest amount of total energy per unit weight. Due to their low capacitance values, electrostatic capacitors are limited to low-power applications, or at most, they are used for short-term memory backup supplies (Sharma and Bhatti, 2010).

The Ragone plot of capacitors exhibits a decreasing slope due to the nature of energy storage in capacitors. Generally, energy storage in capacitors occurs through the accumulation of positive charges within the capacitor, resulting in electrostatic energy. This form of energy is less stable and can be stored in smaller quantities compared to the energy stored in batteries or supercapacitors. When a capacitor is discharged to provide energy in the form of an electrical current, the accumulation of electric charge within the capacitor decreases. Consequently, the electrostatic energy within the capacitor decreases as well. Typically, the rate at which the electrostatic energy decreases results in a decreasing slope in the Ragone plot, reflecting the gradual reduction in stored energy as the capacitor is used.

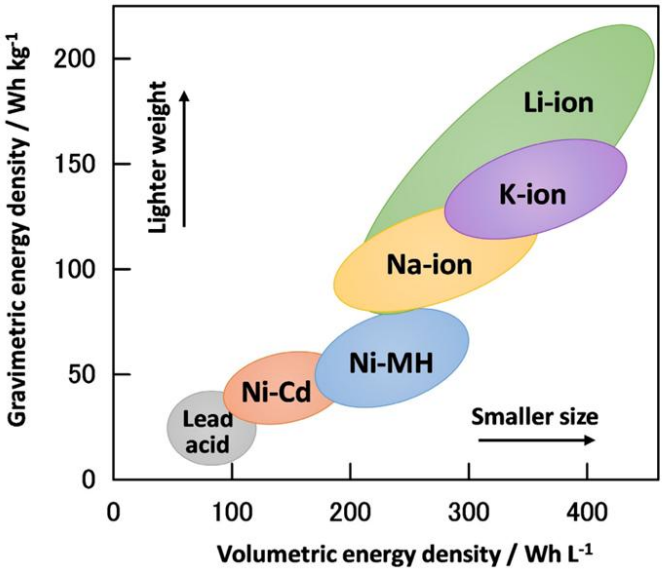

Figure 2.2 Volumetric and gravimetric energy densities of commercial batteries (lead-acid, Ni-Cd), Ni-MH, Na-ion, K-ion, and Li-ion batteries) (Kubota, Dahbi, Hosaka, Kumakura, and Komaba, 2018).

2.2 Batteries

There are various types of batteries, each with distinct features and applications, ranging from everyday devices to those commonly found in smartphones and laptops. These battery types include lead-acid, nickel-cadmium (Ni-Cd), nickel-metal hydride (Ni-MH), sodium-ion (Na-ion or NIBs), potassium-ion (K-ion), and lithium-ion batteries (Figure 2.2). This diversity of battery types enables us to efficiently meet various energy storage needs. Each type has specific advantages and limitations in terms of energy density, cost, cycle life, and environmental impact, making them suitable for different applications.

2.2.1 Lead acid batteries

Lead Acid Batteries are a well-established and widely used energy storage technology known for their reliability and low cost. These batteries operate through a chemical reaction between lead dioxide and sponge lead, producing electrical energy. They find applications in various fields, from automotive vehicles to uninterruptible power supplies, owing to their ability to deliver high current and provide a dependable source of energy (Christen and Carlen, 2000). While newer battery technologies have emerged, lead-acid batteries continue to play a significant role in the energy storage landscape, particularly in applications that prioritize cost-effectiveness and robustness.

2.2.2 Nickel-Cadmium (Ni-Cd) batteries

Nickel-Cadmium Batteries, also known as NiCad batteries, have been a prominent energy storage solution for several decades. These rechargeable batteries use nickel oxyhydroxide (NiOOH) as the cathode and cadmium metal (Cd) as the anode, typically delivering an on-line voltage of 1.2V. In industrial applications, Ni-Cd batteries are a close second to lead-acid batteries, primarily due to their exceptional performance in low-temperature conditions, flat discharge voltage, long lifespan, low maintenance requirements, and overall reliability (Christen and Carlen, 2000). However, a notable drawback is their capacity loss when partially discharged and recharged. To maintain their efficiency, Ni-Cd cells should be fully discharged to zero volts before recharging. Over time, environmental concerns have led to a decline in Ni-Cd battery usage due to the cadmium content, with many users transitioning to more environmentally friendly battery technologies (Kubota et al., 2018).

2.2.3 Nickel-Metal Hydride (Ni-MH) batteries

Nickel-Metal Hydride Batteries have gained prominence in the realm of rechargeable power sources. Their appeal lies in the higher energy density they offer in comparison to traditional nickel-cadmium (Ni-Cd) batteries. This increased energy storage capacity has made Ni-MH batteries a preferred choice for various applications, ranging from portable electronic devices to hybrid electric vehicles. Notably, Ni-MH batteries are celebrated for their eco-friendliness, extended cycle life, and reduced susceptibility to memory effects, making them a reliable and versatile power solution in a world increasingly driven by portable electronics and clean energy technologies (Christen and Carlen, 2000).

2.2.4 Potassium-ion batteries

Potassium-ion batteries, are gaining attention as a potential alternative to lithium-ion batteries for energy storage. These batteries use potassium ions for charge and discharge processes. Unlike lithium, potassium is abundant and cost-effective, which makes K-ion batteries an attractive option for large-scale energy storage applications. While they are still in the development stages and face certain technical challenges, such as electrode materials and overall performance, their potential for addressing the growing demand for energy storage in renewable energy systems and electric vehicles makes them a subject of increasing research.

2.2.5 Lithium-ion batteries

Lithium-Ion Batteries often abbreviated as Li-ion batteries, have revolutionized the world of portable electronics and electric vehicles. They are known for their high energy density, lightweight design, and ability to provide reliable, long-lasting power. The fundamental chemistry of Li-ion batteries involves the movement of lithium ions between the positive and negative electrodes during charge and discharge cycles. These batteries have become the preferred choice for a wide range of applications, from smartphones and laptops to electric cars and renewable energy storage systems, due to their efficiency and adaptability (Christen and Carlen, 2000).

Having high Volumetric and Gravimetric energy densities means that the battery has a greater capacity to store energy. It is lightweight and small. One important reason

why batteries are small and lightweight is a good thing is that they allow for efficient use and high power in tight spaces.

2.3 Glass Batteries

This section serves as a summary of the literature review, focusing on topics relevant to the current research. It covers aspects of glass batteries, including their history, definitions, and structure. Additionally, the use of lithium glass as the cathode material in the batteries under study is discussed. Finally, the section concludes with an overview of glass production techniques.

2.3.1 History of glass batteries

The battery was created by John B. Goodenough, a 97-year-old materials scientist, solid-state physicist, and professor of mechanical engineering and materials science at the University of Texas at Austin (well-known for creating the lithium-ion battery). Batteries comprise three basic components: an anode, a cathode, and an electrolyte. Most batteries have a liquid separator (electrolyte), but glass batteries are entirely solid, making them less dangerous and posing a lower risk of catching fire. These "glass batteries" (the electrolyte was based on a glass powder) have a two-times greater energy density than conventional lithium-ion batteries.

Although it has great and versatile features, this battery technology still faces many challenges to develop and improve its performance. For example, there are not enough suitable solid-state electrolytes (SSEs), and there is also a large interfacial resistance with insufficient interfacial ion/electron transport kinetics. One of the alternatives for improving SSBs' performance is improving cathode materials, as the total achievable capacity of SSBs is determined by the cathode materials.

Recent research focuses on overcoming these limitations by exploring different solid-state electrolyte materials, such as sulfides, oxides, and phosphates, which exhibit improved ionic conductivity. Additionally, there is ongoing work to address interfacial stability, including the development of coatings for cathodes to reduce resistance at the interface. The search for more stable, high-capacity materials like lithium-rich layered oxides, spinel-based cathodes, and even the use of lithium metal

as an anode are seen as crucial steps toward enhancing the energy density, cycle life, and overall safety of solid-state batteries. If these challenges are successfully addressed, glass batteries could revolutionize the energy storage industry, offering safer, more durable, and higher-performance alternatives to traditional lithium-ion batteries (Zhao et al., 2019).

2.3.2 Definition of glass

Glass, with its unique properties including optical transparency, structural strength, and durability, has been a part of human civilization for millennia. Its versatility has led to diverse applications, ranging from advanced technologies like laser glass, optical fibers, and solar glass to everyday items such as glass water containers, bottles, and decorative glass clocks. Additionally, glass plays a role in cutting-edge fields like renewable energy and electronics, where it is used as an electrode in batteries (Karmakar, 2017). It is imperative to know the relationships between different types of glasses.

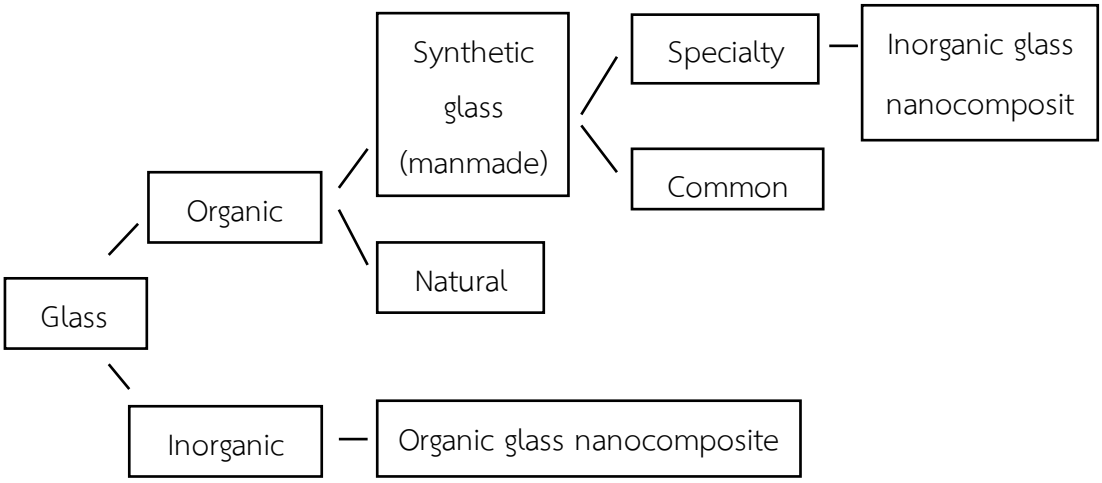

Figure 2.3 The relationships of different types of glasses (Karmakar, 2017).

Figure 2.3 illustrates the classification of glass based on its chemical composition, resulting in two primary categories: inorganic and organic glasses. Inorganic glasses can further be categorized into natural glasses, like obsidian or pechsteins, found in volcanic rocks, and synthetic glasses, which are human-made through the melting of

raw materials and manufacturing processes. Synthetic glasses, in turn, can be divided into two subcategories: common and specialty glasses. Common glass, which includes items like windows, tumblers, bottles, lamps, spectacles, mirrors, and more, serves every day, general purposes (Karmakar, 2017).

2.3.3 Structure of glass

Numerous structural theories have been proposed to explain glass formation. These theories include Goldschmidt's radius ratio criterion and Zachariasen's random network theory, which focus on coordination numbers. Smekal's mixed bonding rule and Stanworth's electronegativity rule, on the other hand, are based on bond type. Sun's single bond strength criterion is rooted in bond strength, while Dietzel's field strength criterion and Phillips' topological constraint model are other relevant models. It's worth noting that some of these theories are now primarily of historical significance and are discussed in detail by Rawson.

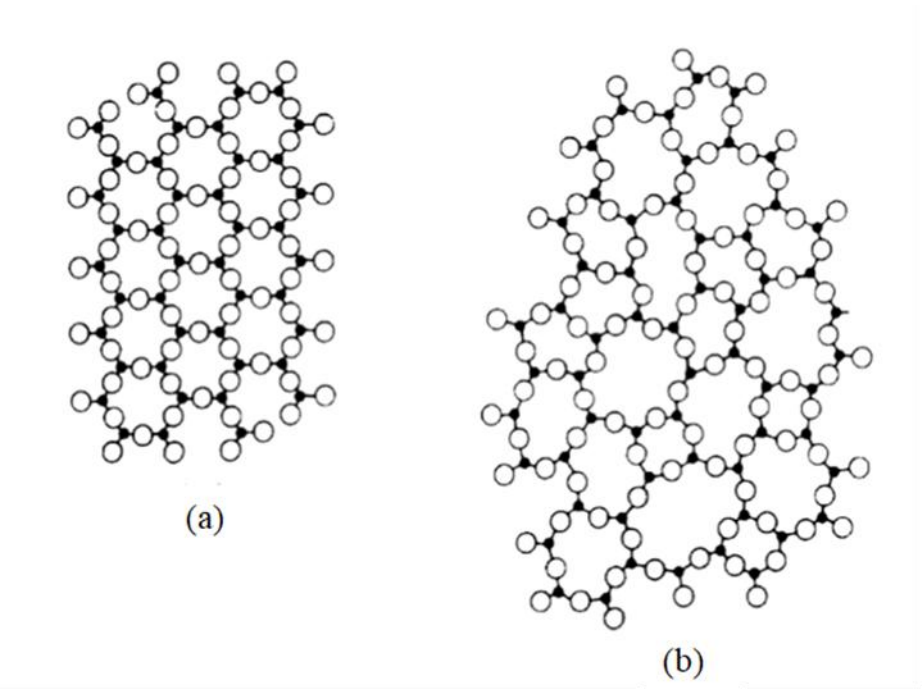

Figure 2.4 Atomic structural representation of (a) A_2O_3 crystal (b) A_2O_3 glass.

In our discussion, we will concentrate on Zachariasen's theory and the latter three models. In a seminal paper that significantly influenced the field of glass science,

Zachariasen put forth a compelling argument. He contended that because the mechanical properties of glasses closely resemble those of their crystalline counterparts, the atomic forces in both materials must be of a similar magnitude. The broad diffuseness observed in x-ray diffraction spectra for glasses strongly implied that glass possesses an extraordinarily large unit cell, forming a three-dimensional random network. Consequently, this randomness leads to glass having higher internal energy compared to crystals. Zachariasen believed that the disparity in internal energy between glass and crystals must be minimal; otherwise, there would be a substantial driving force towards crystallization. Additionally, he suggested that this slight energy difference necessitates an open and flexible atomic structure for glass.

In ionic crystals, it's common for the cation polyhedra to share corners. This is especially the case when dealing with cations that have a small radius but a high charge. Zachariasen proposed that sharing corners is a fundamental requirement for achieving a structure that is both open and random. So, if we imagine a hypothetical compound like A_2O_3 crystallizing in two dimensions, the atomic arrangements in both the crystalline and glassy forms should resemble what's depicted in Figure 2.4. In both cases, you'll see triangles made up of AO_3 units connecting at their corners (Varshneya, 2013). However, in the glassy form, there's an element of disorder due to variations in the A-O-A bond angles (referred to as bond angles) and slight changes in the A-O bond lengths. It may also be noted that the triangles or the O-A-O angles themselves need not be deformed much (Varshneya, 2013).

2.3.4 Glass on battery electrode

The preference for using lithium-ion batteries over silica as glass on battery electrode is due to several reasons. Lithium-ion batteries offer higher energy storage capacity, lighter weight, better efficiency in energy storage and release, and greater durability in various environmental conditions. They also provide better control and dissipation of heat, reducing the risk of fire and other hazardous incidents. Additionally, lithium-ion batteries have a longer lifespan and lower energy loss during operation, making them more advantageous for applications requiring safety, efficiency, and lightweight properties.

Crystalline materials have been widely utilized as cathode materials for lithium-ion batteries (LIBs), but they face limitations related to factors like symmetry, phase transitions, crystal orientation, and cost. The development of high-capacity crystalline materials is often constrained. Amorphous electrode materials, on the other hand, show promise with their short-range ordered structure, high surface area, and free volume, allowing for lattice distortion without macroscopic phase transitions and thus improving kinetics. Several studies indicate that amorphous electrodes exhibit enhanced cyclic performance and higher capacity compared to crystalline electrodes (Wei et al., 2018).

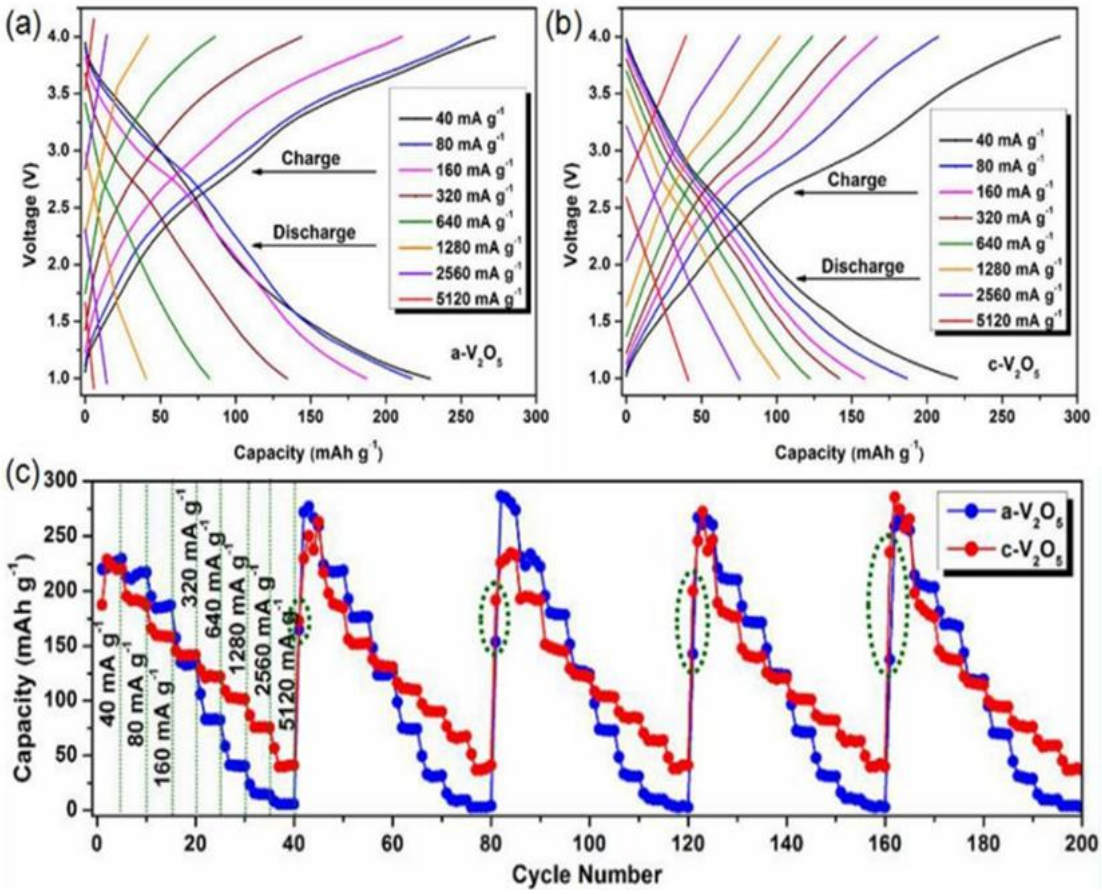

Figure 2.5 The galvanostatic discharge/charge curves for two types of V_2O_5 cathodes, a) amorphous (a-V_2O_5) and b) crystalline (c-V_2O_5), were recorded at different current densities within the voltage range of 1.0 to 4.0 V. Additionally, c) comparison of the rate performance between these two cathodes (Liu et al., 2016).

In the following section, we will review various research works that have successfully employed glass materials for use in the electrodes of batteries. These studies have significantly contributed to enhancing the performance and efficiency of electrochemical energy storage systems. By exploring the latest advancements in glass battery technology, we can gain insights into the promising innovations that may shape the future of energy storage solutions.

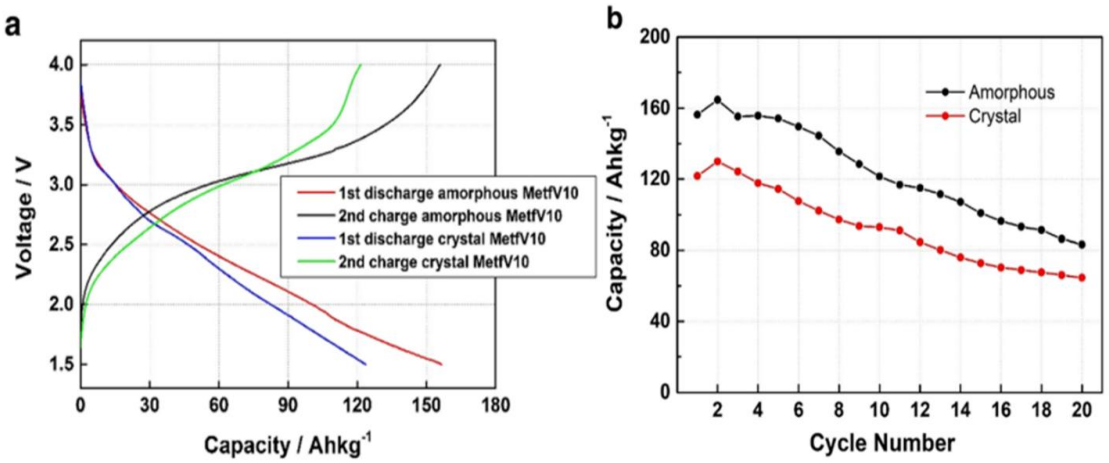

Figure 2.6 a) First discharge and second charge curves of LIBs using amorphous and crystal MetfV10 cathodes. b) Cycle performance of LIBs using amorphous and crystal cathodes (Wang, Isobe, Matsumura, and Yoshikawa, 2018).

In 2014, Shikun Liu and a team conducted a comparative analysis of amorphous and crystalline V_2O_5 cathodes in sodium-ion batteries. They created amorphous V_2O_5 (a-V_2O_5) cathodes by subjecting V_2O_5 samples to drying at 120°C for 10 hours in a vacuum chamber. Subsequently, they annealed these cathodes at 350°C for 4 hours in an air environment to form crystalline V_2O_5 (c- V_2O_5) cathodes. The results showed that a-V_2O_5 cathodes exhibited higher reversible capacities at low current densities (217.1 and 186.9 mAh/g at 80 and 160 mAh/g, respectively) compared to c-V_2O_5 cathodes (186.6 and 158.3 mAh/g), as depicted in Figure 2.5c. In contrast, the cathode composed of c-V_2O_5 exhibits superior specific capacities compared to the cathode composed of a-V_2O_5 under conditions of high current densities. The electrochemical findings presented in this study demonstrate that amorphous materials possess

notable characteristics that make them a compelling choice for utilization as cathode materials, particularly under conditions of low current densities (Liu et al., 2016).

Moreover, in 2018, Heng Wang and his group reported on the properties of amorphous and crystalline cathode materials for lithium-ion batteries. In Figure 2.6, the electrochemical performance of the amorphous and crystalline MetfV10 cathodes was systematically investigated. The galvanostatic discharge and charge curves of the two different (Figure 2.6a) cathodes showed that the discharge capacities of the amorphous and crystalline MetfV10 cathodes in the first discharge were 156 and 122 mAh/g, respectively. Moreover, Figure 2.6b shows the cycle dependence of the discharge capacities for the two cathodes. It can be clearly seen that the amorphous cathode maintains a capacity greater than the crystalline cathode (approximately 100 mAh/g after 20 cycles). The disordered structure of the amorphous cathode may help Li ions more easily intercalate into the materials, resulting in a decrease in resistance. These results show that amorphous materials are a good candidate to replace or develop cathode materials (Wang et al., 2018).

2.3.5 Glass production

Currently, there are a range of techniques for creating glass, such as melt-quenching, sol-gel, chemical vapor deposition, sputtering, and others. The melt-quenching method is widely used because of its simplicity, ease of use, and suitability for producing various types of glass in small-scale laboratory settings. In light of the information presented above, the following discussion will proceed as follows:

2.3.5.1 Melt-quenching technique

The melt-quenching technique, a widely employed method in materials science and glass manufacturing, involves the melting of raw materials or glass precursors. Once molten, the glass is rapidly cooled to solidify, resulting in a transparent and non-crystalline material. This technique is valued for its simplicity and adaptability to small-scale production, making it a pivotal process for crafting various glass compositions and shapes, particularly in research and laboratory settings.

The Melt-Quenching Technique has been extensively investigated for the production of lithium borate glass, and it is the primary method employed in

creating most types of glass today. This process involves heating the raw material mixture, or batch, to temperatures ranging from 1100 to 1600°C, followed by controlled melting for a specific duration. After casting, any residual thermal stresses are eliminated through an annealing process conducted near the glass transition temperature of the respective glasses, resulting in what are known as "as-prepared glasses." To prepare these as-prepared glass samples for various characterization methods, they are typically sawed, ground, and polished.

The initial steps involve selecting suitable raw materials and then preparing the batch through chemical calculations, weighing, and thorough mixing. The uniformity of the glass melt is maintained by periodically stirring it with a platinum or silica glass rod. Glass melting crucibles can be crafted from a range of materials, including fused silica (SiO_2), alumina (Al_2O_3), pure platinum (Pt), oxide-dispersed-strengthened (ODS) platinum, platinum-gold (Pt-5% Au), platinum-rhodium (Pt-10% Rh), or platinum-iridium (Pt-10% Ir). To prevent contamination, it is advisable to use pure platinum (Pt) or ODS platinum crucibles. Appropriate caps can be employed to slow the rate of evaporation loss.

2.3.5.2 Sol-Gel Method

The sol-gel method has gained increasing official recognition as a primary technique for glass fabrication. This wet-chemical approach utilizes liquid sources to synthesize both inorganic materials and organic-inorganic hybrids, making it a preferred method in various research and industrial settings. Silicate systems, particularly, have been extensively explored within the sol-gel synthesis framework due to the availability of molecular silicon sources like tetra alkoxysilanes, which offer moderate reactivity. By undergoing hydrolysis and polycondensation reactions, these compounds yield silica gels, which can be converted into silica glasses at relatively low temperatures (around 1000–1500°C) without melting. This process, devoid of melting, is gaining official recognition due to its numerous advantages over conventional methods. It allows for enhanced dopant concentration, broader compositional range, and tailored photo- and magnetoactive centers within the glass

structure. Despite challenges, such as the tendency of sol-gel-derived wet gels to fracture during drying, efforts to refine techniques and overcome obstacles are steadily improving. Consequently, the sol-gel method is becoming increasingly institutionalized as a pivotal approach in the fabrication of monolithic silica glasses and specialized functional glass compositions (Kajihara, 2013).

2.3.5.3 Chemical Vapor Deposition

The Chemical Vapor Deposition (CVD) technique for glass is an official and established method used to deposit thin films or coatings onto glass substrates. It involves the chemical reaction of gaseous precursors to form a solid material on the surface of the glass. The CVD process typically requires precise control over temperature, pressure, and gas flow rates to achieve the desired deposition characteristics. This method is commonly employed in industries requiring high precision and performance, such as optical coatings, semiconductor manufacturing, and electronics. CVD offers advantages like uniform thickness distribution, excellent adhesion, and the ability to deposit complex materials with tailored properties. As a result, it has become an increasingly institutionalized approach in the fabrication of advanced glass products for various applications (McCurdy, 1999).

2.3.5.4 Sputtering Method

The Sputtering method, employed for glass applications, involves the deposition of thin films or coatings onto glass surfaces through a process known as physical vapor deposition (PVD). This technique utilizes high-energy ions to dislodge atoms from a target material, which then deposit onto the glass substrate, forming a thin film. Taking advantage of a vacuum environment, the sputtering process allows for precise control over film thickness, composition, and structure. Widely utilized across various industries, including electronics, optics, and automotive, sputtering enables the creation of functional coatings such as transparent conductive layers and anti-reflective coatings. Its versatility and capability to enhance the properties of glass

make sputtering a pivotal method in modern glass fabrication and technological advancements (Stan et al., 2023).

2.4 Characterization techniques

In this section, we will delve into the characterization techniques employed in this study. Specifically, one of the key techniques utilized for measurement and analysis is XRD.

2.4.1 X-ray diffraction (XRD)

X-ray diffraction is a crucial technique for studying the atomic and molecular structure of materials. It is widely used in scientific fields like chemistry, physics, and materials science to reveal the arrangement of atoms in crystal lattices. XRD helps determine the crystallographic properties of various substances by measuring X-ray scattering angles and intensities, providing valuable insights into material structures. This technique has been pivotal in uncovering the structures of many compounds, enhancing our understanding of matter's properties.

The present chapter first presents a condensed overview of the generation of X-rays as well as the theory of diffraction of X-rays by crystals. Subsequently, the methods for analyzing X-ray patterns of both amorphous and crystalline materials are presented.

During the war years, extensive research was conducted to quantify radiation dosage, with a particular focus on X-ray spectra. In 1912, the x-ray diffraction experiment, which revealed x-rays as electromagnetic waves, garnered significant attention in the scientific community. Max von Laue, a Nobel Prize laureate, presented a compelling synthesis of evidence supporting both the electromagnetic radiation model and the particle-like explanation. The Bragg father-and-son duo, using x-rays as a crystallographic tool, confirmed that x-rays are electromagnetic waves capable of interfering with lattices, providing atomic-scale information about crystal structures inaccessible to visible light. This pioneering technique led to the first images enabling the inference of atomic structures in solids (Kitaigorodsky, 2012), which was established

in the early 20th century. The Braggs demonstrated a remarkable ability to precisely characterize fundamental structures, including that of common substances like rock salt (NaCl) (Borisov and Podberezskaya, 2012). The examination of X-ray intensities reflected by crystals further substantiated Niels Bohr's atomic model and the concept of chemical bonding (Sheldrick, 1998).

In the past few decades up to the present day, X-ray analysis techniques have been employed to accurately determine the distances between atoms and their arrangement in various substances. These techniques have found applications in numerous scientific disciplines.

2.4.1.1 Principle of X-ray diffraction

In this section, we will provide an overview of the fundamental principles of X-ray diffraction (XRD) techniques.

X-rays, characterized by wavelengths between 10^{-3} and 10^{1} nanometers (Spieß, Behnken, Genzel, Schwarzer, and Teichert, 2009), are typically produced using sealed tubes and rotating anodes. In this process, electrons are generated by heating a tungsten filament within a vacuum. These electrons are subsequently accelerated through a high electric potential field and focused on a target material, resulting in the emission of X-rays. Incident electrons generate X-rays through two mechanisms: first, the deceleration of electrons results in the emission of X-ray photons, producing a continuous spectrum known as Bremsstrahlung (Schwartz and Cohen, 2013). Second, when atoms are ionized by incoming electrons, inner-shell electrons are ejected, and outer-shell electrons fill the resulting gaps. The energy difference between these electron transitions leads to the emission of characteristic X-rays with energy levels specific to the material (Epp, 2016).

The methods are fundamentally founded on the diffraction of X-rays by regularly spaced atomic planes and the detection of the diffracted signal in terms of either angle or energy. The geometric interpretation of X-ray diffraction, based on constructive interferences, was initially expounded by W.L. Bragg in 1913 (Bragg and Thomson, 1914). Bragg's solution to X-ray diffraction views it as the reflection of X-rays

from the atomic planes of a crystal, following the laws of reflection. A crystal with Miller indices [hkl] is considered a series of parallel atomic planes separated by a distance d. Figure 2.7 details the geometric conditions for diffraction and the derivation of Bragg's law (Equation 2.1).

$$n\lambda = 2d_{hkl}\sin(\theta) \qquad \text{Equation 2.1}$$

In Equation 2.1, 'n' represents the order of diffraction, 'λ' denotes the wavelength of the incident beam in nanometers (nm), 'd_{hkl}' signifies the lattice spacing in nanometers, and 'θ' corresponds to the angle of the diffracted beam in degrees.

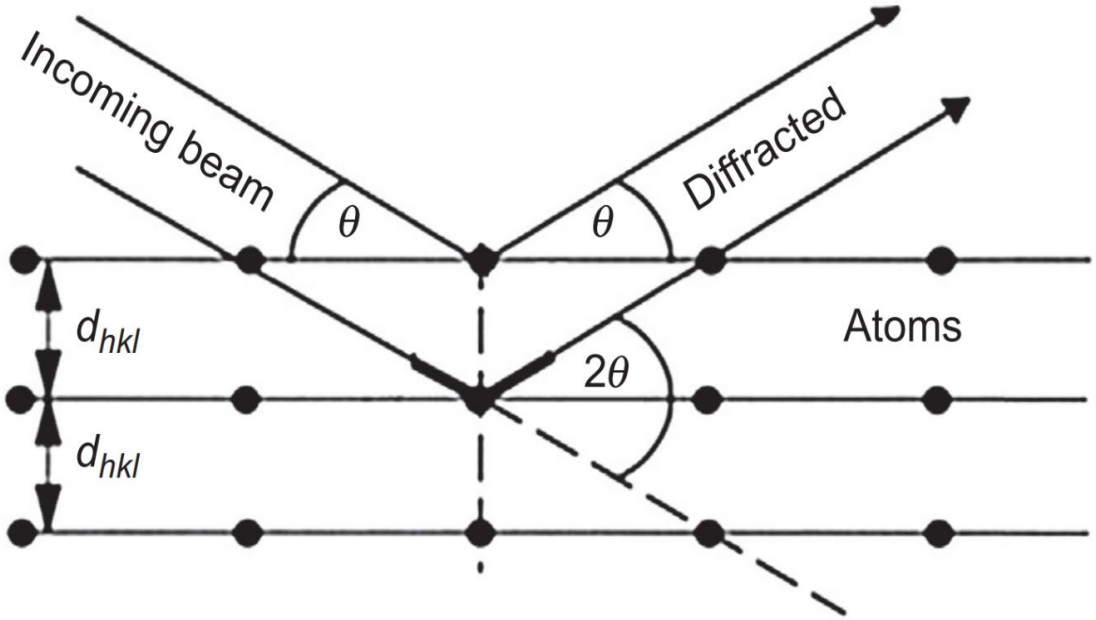

Figure 2.7 A simplified model of the Bragg equation (Epp, 2016).

Crystals are ordered arrangements of atoms, and X-rays can be thought of as electromagnetic radiation waves. When X-rays hit a crystal, the atoms scatter them, mostly because the rays interact with the atoms' electrons. Elastic scattering is the name given to this process, in which the electron plays the role of the "scatterer." When scatterers are arranged regularly, the resulting spherical waves also behave

predictably. In most directions, these waves cancel each other out through destructive interference, but in a few, as determined by Bragg's law (Equation 2.1).

For this expression, the wavelength is denoted by lambda, the distance separating atomic planes by d, and the angle of incidence of the X-ray beams by theta, where n is an integer (1, 2, 3,...n). Because it "reflects" off an adjacent atomic plane, an X-ray beam travels in a more circuitous (but still parallel) path. It is necessary for the incident X-ray beams to have a path length difference of exactly 1 for constructive interference to occur and a strengthened diffracted beam to be produced (Epp, 2016).

2.4.1.2 Phase identification of X-ray diffraction

The building blocks of a crystal are repeated patterns (Figure 2.8d) that are ordered in three dimensions. However, atoms in amorphous materials are scattered randomly throughout three dimensions (Figure 2.8b), so they lack periodicity. This scenario calls for attention to X-ray scattering by atoms. X-rays will scatter in only certain directions when they hit the lattice planes due to the periodic arrangement of the atoms (formed by atoms). Extremely bright peaks will result from this (the width of the peaks depends on other variables). In the amorphous state, X-rays scatter in many directions, producing a broad, uneven peak (2 theta) rather than concentrated high-intensity peaks. If there is enough amorphous phase to give a peak, then you will get the peaks of the relevant phase, but they will not be sharp, because an XRD pattern is composed of the sum of the contributions of all constituent phases. It's possible that a higher proportion of the amorphous phase will appear in the diffraction pattern if the experiment is conducted at a low angle. A sharp peak of the crystalline phase's preferred orientation and a fuzzy peak of the amorphous phase's strongest peak will be visible if both phases have peaks. As a result, the amorphous phase will only show its strongest peak once. The second peak, if present, may be discernible if its intensity is sufficiently high, but the contrast between them will be low (Figure 2.8a,c) (Epp, 2016; Nunes, Mahendrasingam, and Suryanarayanan, 2005).

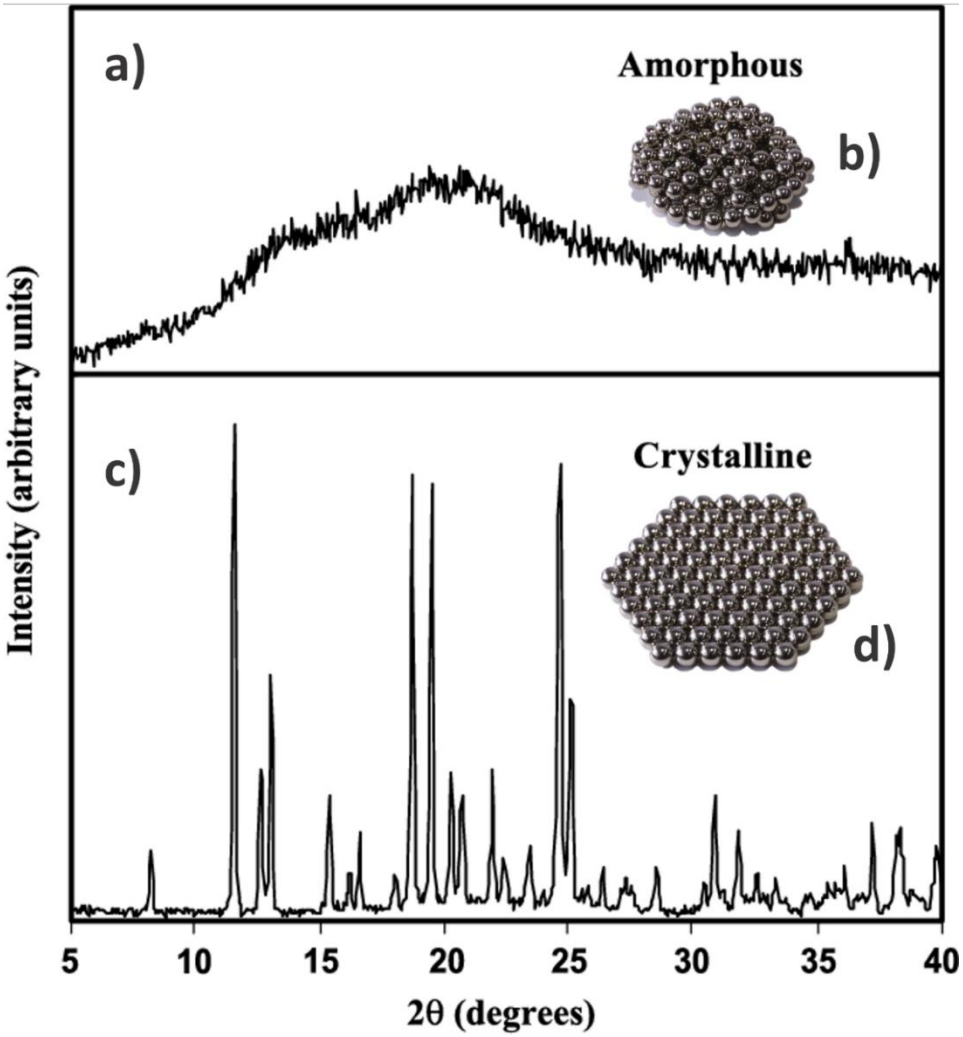

Figure 2.8 The XRD patterns of a) amorphous and c) crystalline forms, along with the crystal structure diagrams of b) amorphous and d) crystalline forms, are presented and summarized (Nunes et al., 2005).

2.4.2 The cyclic voltammetry (CV)

Cyclic voltammetry (CV) is used to examine the energy generated in batteries or other energy storage devices by measuring the current flowing through the energy-setting component (electrode) in the device being tested. The key feature of CV is its ability to measure energy in various forms over time. Applying a square wave voltage, allows observation of changes in current over time, aiding in the assessment of energy occurring in the device during specific operational periods. CV measurements help improve the understanding of the behavior of energy storage devices.

2.4.2.1 Principles of cyclic voltammetry

Cyclic voltammetry is a cornerstone technique in electrochemistry, utilized to investigate the fluctuations in electrical current passing through a resistor as the potential of an electrode varies at a designated temperature and pressure. This analytical method is frequently employed to study the electroactivity of substances undergoing chemical transformations during an electric current. Widely utilized in research and development, especially in the realms of organic chemistry, materials science, and biotechnology, cyclic voltammetry offers insights into the electrochemical behavior of various substances on an atomic scale. By systematically altering the potential within predefined limits, and oscillating between positive and negative values, cyclic voltammetry generates data that reveal the electrochemical properties of the substance under scrutiny. Analyzing the resulting cyclic voltammogram enables the prediction of the electrode's capacitive attributes and identification of redox peaks corresponding to reduction and oxidation processes. Through this method, the substance's oxidation and reduction potentials can be determined with precision and accuracy (Choudhary, Jothi, and Nageswaran, 2017).

Cyclic voltammetry is rooted in the principle of linear sweep voltammetry, a method that tracks current while linearly sweeping potential over time. The rate of voltage change, known as the scan rate (m s-1), characterizes this technique. Linear sweep voltammetry yields diverse outcomes influenced by factors such as the rate of electron transfer, electrochemical reactivity of materials, and the chosen scan rate. Results typically manifest as either anodic or cathodic peaks, depicted in Figure 2.9a. While similar to linear sweep voltammetry, cyclic voltammetry diverges by not concluding with a single sweep within a fixed voltage range. Instead, it cyclically returns from E2 to E1 after reaching the endpoint. This cyclical behavior gives rise to the term "cyclic," with the resulting current versus voltage plot termed a 'cyclic voltammogram', as illustrated in Figure 2.9b. In cyclic voltammetry, the scan rate (v) is a pivotal parameter. Voltage sweeps from E1 to E2, representing the slope of a linear voltage change during measurement. Repeating multiple cycles under consistent conditions provides additional insights into voltage, reversibility, and cyclability of

redox reactions. Furthermore, adjusting the scan rate allows for the investigation of electrochemical redox reaction kinetics.

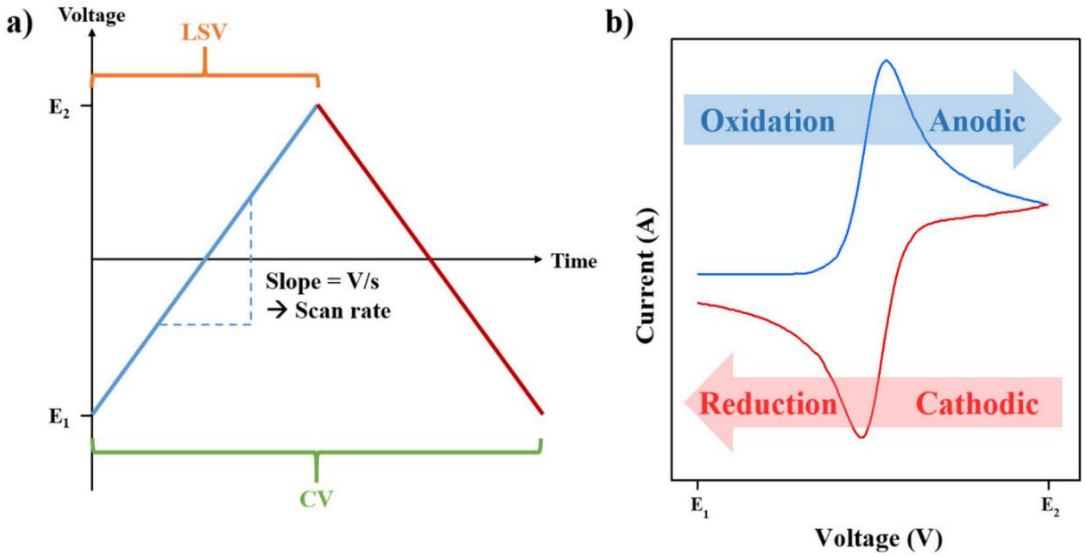

Figure 2.9 a) The voltage versus time profile distinguishes between linear sweep and cyclic voltammetry. b) A standard cyclic voltammogram illustrates both cathodic and anodic peaks (Kim et al., 2020).

For the differential capacity (dQ/dV) plot, it is recorded based on a similar principle as the cyclic voltammogram. Although it provides useful information on the redox reactions of electrochemical systems, the difference between the cyclic voltammogram and the dQ/dV plot should be recognized, as the cyclic voltammogram contains rate information. In general, the current (I) is plotted on the y-axis versus the voltage (V) on the x-axis in the cyclic voltammogram, and it can be transformed into a dQ/dV plot. For the transformation of a cyclic voltammogram to a dQ/dV plot, the I and V can be expressed as.

$$V = vt \qquad \text{Equation 2.2}$$

$$dt = \frac{dV}{v} \qquad \text{Equation 2.3}$$

$$I = \frac{dQ}{dt} \qquad \text{Equation 2.4}$$

where v is scanning rate (Vs^{-1}), V is the voltage (or potential, V), I is the current (A), Q is charge stored (Ah), and t is time (s). And the formula 2.5 which indicate the y-axis of dQ/dV plot was obtained by combining the equation 2.3 and 2.4

$$\frac{I}{v} = \frac{dQ}{dV} \qquad \text{Equation 2.5}$$

Moreover, it is necessary to understand the different experimental conditions between galvanostatic cycling (charge-discharge) and CV in terms of a driving force for electrochemical reactions; the potential increases linearly with time in CV, whereas the current is maintained during galvanostatic cycling. Regardless of state of charge (SOC) of the working electrode, these forced changes in potential increase.

The current beyond the operating limits of the cell. Thus, it would be difficult to make a comparison of accessible capacity. In addition, the IR drop of the cell remains consistent during the constant current scan, which depends on the CV sweep, so the peak position and shape can be changed as shown in Figure 2.10. Therefore, before using dQ/dV plot, it is necessary to understand the commonalities and differences between CV and dQ/dV (Kim et al., 2020).

The CV experiment can be performed with a single cycle or with numerous cycles of varying voltage. The scan rate is defined as the slope of the ramp signal in volts per unit time. This scan rate can vary from a few hundredths of a millivolt per second to tens of thousands of volts per second. To better understand the cell's electrochemistry, the scan rate can be adjusted. Therefore, the test sample's voltametric behavior is highly dependent on the scan rate. It is reasonable to anticipate that the oxidation and reduction peak currents and peak potentials will vary with the scan rate. A good rate capability and improved pseudocapacitive behavior of the electrode material are both indicated by an increase in the peak current (faradaic current) with an increase in the scan rate. The presence of the electroactive species at the surface of the electrode (the working electrode) causes a greater number of redox reactions as the scan rate increases. However, if the scan rate is too slow, the products of the reduction or oxidation can take part in a chemical process whose products may not be electroactive, and the peak (either the forward or reverse scan peak) would be

missed. It is possible to determine this peak current in the CV by utilizing the Randlese-Sevcik equation:

$$I_p = 2.69 \times 10^5 \, n^{\frac{3}{2}} AC\sqrt{vD} \qquad \text{Equation 2.6}$$

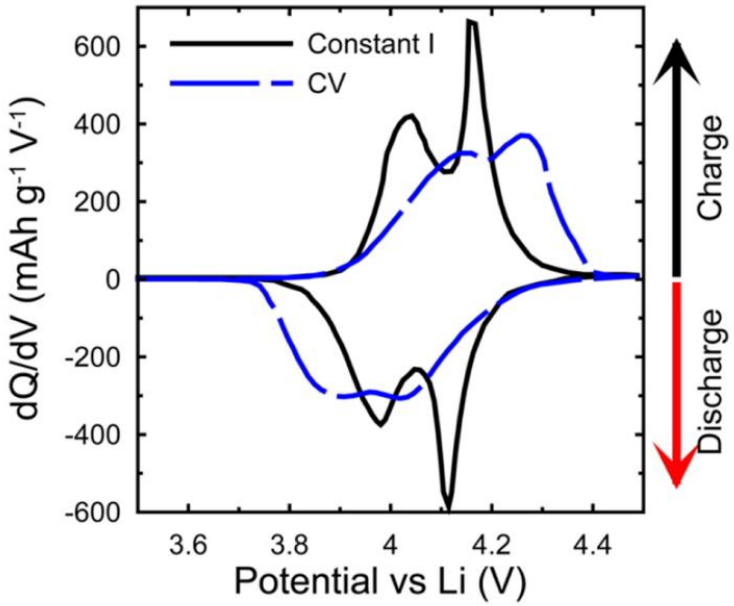

Figure 2.10 CV and dQ/dV curve of $Li_xMn_2O_{4+}\delta$ vs Li metal with constant current experiment as C/8 = 0.33 mA/cm^2 and CV: 0.04 mV/S (sweeps up and down in 6.9 h). Reprinted with permission (Potyrailo and Maier, 2006).

where I_p denotes the peak current, n refers to the number of electrons in the redox reaction, A indicates the area of the working electrode, C signifies the concentration of the electroactive species at the electrode, v represents the scan rate, and D denotes the diffusion coefficient of the electroactive species. Each of these factors is critical in establishing the peak current in CV (Choudhary et al., 2017).

Capacitance is measured at varying sweep speeds to provide a comprehensive picture of its behavior in the CV. In addition, the following formula can be used to estimate the material precise capacitance:

$$C_s = \frac{\int IdV}{vm\Delta V} \qquad \text{Equation 2.7}$$

where ΔV is the potential window (V), m is the mass of electroactive material (g), v is the scan rate (mV/s), and $\int$ IdV is the area under the curve in the plot of I versus V.

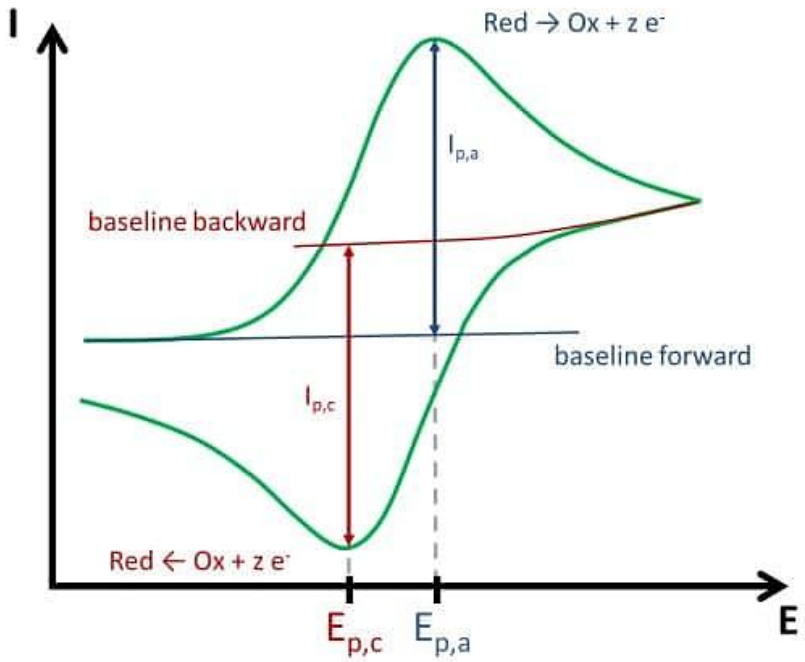

Figure 2.11 The CV of a freely diffusing reversible species, together with an indication of the peak currents and peak potentials for the anodic and cathodic peaks.

A cyclic voltammogram involves regulating the voltage and monitoring the current. The potential for either growth or decay is linear. The scan rate v is the rate of change of the potential over time. Mathematically speaking, this corresponds to the slope of the linear potential (see equation 2.8).

$$V = \frac{\partial E}{\partial t} \qquad \text{Equation 2.8}$$

Potentials at the outset are often inactive, meaning no electrochemical reaction is taking place. In most cases, the linear sweep of the potential will cross the formal potential of the species under study (Figure 2.11). After a certain threshold is crossed, the slope of the linear potential flips, such that a negative potential becomes

a positive one and vice versa. The vertex potential is the name given to this potential. When the potential returns to its initial value, the cycle is complete.

This procedure may be repeated as often as desired. The purpose of performing several cycles is to gauge the robustness of a system. In most modern software, the potential sweeps between the two vertex potentials and begins at a potential between these two, with the opportunity to specify a start potential in between.

2.4.2.2 The shape of a cyclic voltammogram

An example CV for a solution with a single freely diffusing reversible species is shown in Figure 2.11. The peak data is read in the same way. The peak information includes the cathodic peak currents Ip, c, and potential Ep, c, as well as the anodic peak current Ip, a. The arrangement of a curriculum vitae can provide a wealth of qualitative data. Either by analyzing the peaks themselves or by monitoring how they evolve over the course of a series of observations, more crucial information can be gleaned. Please be aware that it is more challenging to establish a baseline for the back scan because the current at the beginning of the back scan incorporates the diffusion-limited current of the forward scan. In this section of the guidelines, you'll find details on how to account for this circumstance. If the peak current is being monitored solely for quantitative analysis purposes, then the baseline offset is irrelevant.

2.4.3 Electrochemical Impedance Spectroscopy (EIS)

Electrochemical Impedance Spectroscopy (EIS) is a powerful and versatile technique used to investigate the electrical properties of materials and the kinetics of electrochemical reactions. EIS is widely employed in various fields, including battery research, fuel cells, corrosion studies, and sensor development. This technique provides detailed information about the electrochemical processes occurring at the electrode-electrolyte interface and within the bulk of the material.

2.4.3.1 Basics of Electrical Impedance Spectroscopy

Impedance spectroscopy is a non-destructive measurement technique that can be used to examine a battery or parts of a battery (e.g. a half-cell, i.e. only the anode). Figure 2.12a shows the basic measurement principle. For the

measurement, the cell is connected at its two poles to an impedance spectroscopy meter. These are offered by various manufacturers such as Biologic or Gamry Instruments. There are different measurement variants, but one of the standard measurement methods is galvanostatic impedance spectroscopy. In this, a sinusoidal alternating current is applied to the cell. A low current is set, since only then does the battery exhibit linear behavior to a first approximation [1]. The alternating current pulse then leads to a phase-shifted voltage response. The behavior follows the basic equations of AC theory. With the current amplitude I0 it results in the following AC time signal:

$$I(t) = I_0 * \sin(\omega t) \qquad \text{Equation 2.9}$$

The voltage of the cell responds to this excitation and accordingly the following phase-shifted AC voltage time signal can be measured:

$$U(t) = U_0 \sin(\omega t + \phi) \qquad \text{Equation 2.10}$$

EIS involves the application of a small, alternating current (AC) signal to an electrochemical system and the measurement of the resulting voltage response. By varying the frequency of the AC signal over a wide range, typically from milli-hertz to mega- hertz, EIS can probe different processes occurring in the system. The impedance (Z), a complex quantity, is calculated as the ratio of the AC voltage (U) to the AC current (I) at each frequency (ω):

$$Z(\omega) = \frac{U(\omega)}{I(\omega)} \qquad \text{Equation 2.11}$$

The impedance is a complex quantity with magnitude and phase shift, both of which depend on the frequency of the signal. In electrochemical systems, the frequency typically ranges from 100 kHz to 0.1 Hz. As mentioned earlier, $Z(\omega)$ is a complex quantity and can be expressed in polar coordinates. The impedance can be written as:

$$Z(\omega) = |Z(\omega)| e^{j\emptyset(\omega)} \qquad \text{Equation 2.12}$$

where ω is the magnitude of the impedance at frequency $\emptyset(\omega)$ and ω is the phase shift at frequency ω. In Cartesian coordinates, impedance can be written as:

$$Z(\omega) = Z'(\omega) + jZ''(\omega) \qquad \text{Equation 2.13}$$

where $Z'(\omega)$ is the real component and $Z''(\omega)$ is the imaginary part at frequency ω with $j = \sqrt{-1}$

With these data it is now possible to calculate the complex resistance (also called impedance) which results from Ohm's law (Figure 2.12b):

The graph showing the relationship between the real and imaginary parts of impedance is called a Nyquist plot, as illustrated in Figure 2.12. The advantage of the Nyquist plot is that it provides a quick overview of the data and allows qualitative interpretation. The axes for the real and imaginary parts are kept equal to avoid distorting the shape of the graph, which is crucial for qualitative analysis. However, the downside of the Nyquist plot is that it does not display frequency dimensions. One way to address this issue is by labeling the frequency values directly on the graph. This impedance spectrum is often displayed in a Nyquist diagram (Figure 2.12c) and serves as the basis for evaluation. In the Nyquist diagram, each point represents a specific frequency, with the real and imaginary parts of the complex resistance plotted on the x and y axes, respectively.

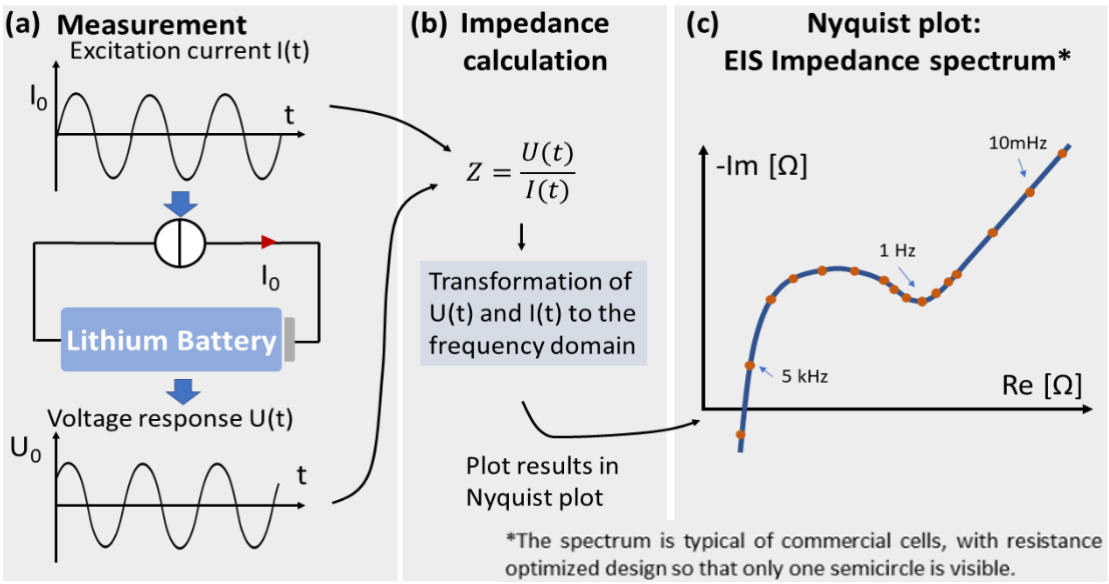

Figure 2.12 Measurement principle for measuring galvanostatic impedance; (b) Conversion of the measured values into impedance; (c) Representation of the measurement results in the Nyquist plot, Own illustration.

2.4.3.2 Electrochemical equivalent circuit

A common method for analysis is the development of an empirical equivalent circuit of the cell, based on the impedance graph, which indicates the internal temperature of the cell. This equivalent circuit typically consists of components such as resistors, capacitors, and possibly inductors. Constructing the equivalent circuit can minimize deviation from the measured impedance spectrum. This approach simplifies the analysis by using various components, as shown in the diagram, which may provide the desired information, such as the structure of the equivalent circuit. A semicircular model is often used in this method, visible on the impedance spectrum, and values can be extracted from the impedance spectrum using simple formulas (as referenced in the work of Choi, W., Shin, H., et al.). Several key parameters can be extracted from EIS measurements:

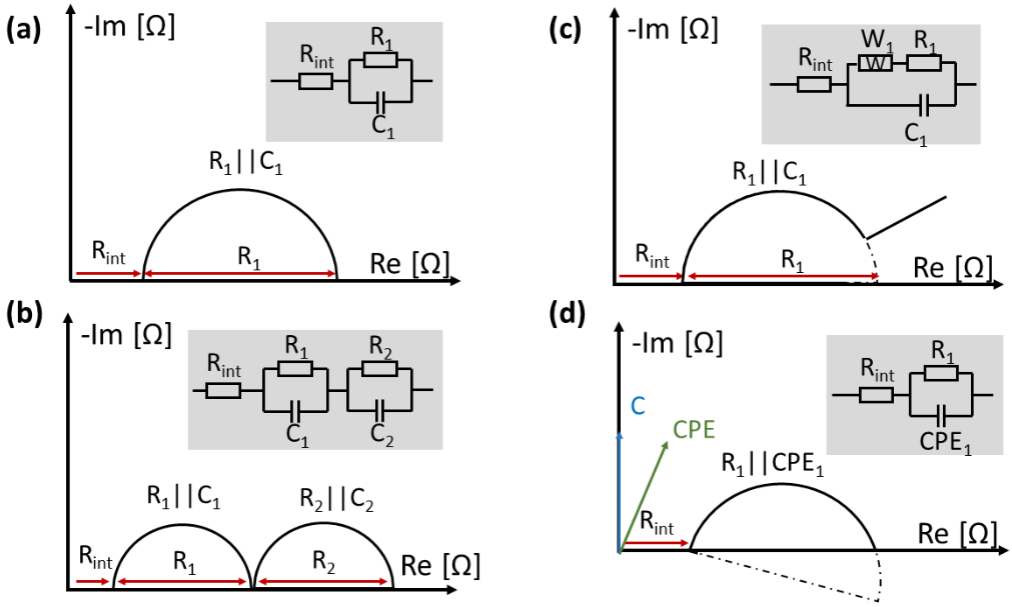

Figure 2.13 The illustration shows different simplified equivalent circuits in the Nyquist diagram: (a) RC components with an additional resistor, (b) a series connection of two RC components and one internal resistor, and (c) an RC component with Warburg impedance and an internal resistor.

- **Solution Resistance (R_s):** Also known as bulk resistance (Rb), this is the resistance of the electrolyte, typically observed at the high-frequency intercept on the real axis of the Nyquist plot.
- **Charge Transfer Resistance (R_{ct}):** This represents the resistance to electrochemical reactions occurring at the electrode surface and often appears as a semicircular arc in the Nyquist plot. Rct increases as the electrode becomes more polarized when the electrode potential is forced to deviate from zero during an open circuit, due to electrochemical reactions, causing current flow at the electrode surface.
- **Constant Phase Element (CPE):** This is an ideal capacitor, assuming the surface properties in the experiment are uniform throughout the system, which is often not the case. Thus, the CPE is used to describe the non-uniform characteristics of the surface.
- **Warburg Impedance (Z_w):** Related to the diffusion of electrochemical species to the electrode surface, it typically appears as a straight line at a 45-degree angle in the low-frequency region of the Nyquist plot. The impedance of some electrochemical cells can result from the adsorption of reactants on the surface, which can be modeled by an inductor. Additionally, inductance may arise from uneven current distribution.

2.4.3.3 Physical models and their evaluation

Figure 2.14 shows the structure of a battery. The anode and cathode each consist of many small grains of active material (for the anode here graphite, for the cathode here LCO) immersed in the liquid electrolyte (For Li-ion batteries). During the discharge process, the lithium moves within a grain at its grain boundary. The lithium deintercalates from the graphite grains and splits into a positively charged lithium ion and an electron. The lithium ion migrates through the porous separator to the cathode with the help of the conducting salt (usually $LiPF_6$). The electron uses conductive soot (carbon black), and migrates via the negative terminal and the connected load to the positive terminal and reaches the cathode this way. At the grain

boundaries of the active cathode particles, the Li-ion and electron react with the cathode. The lithium is then deposited between the cobalt oxide layers.

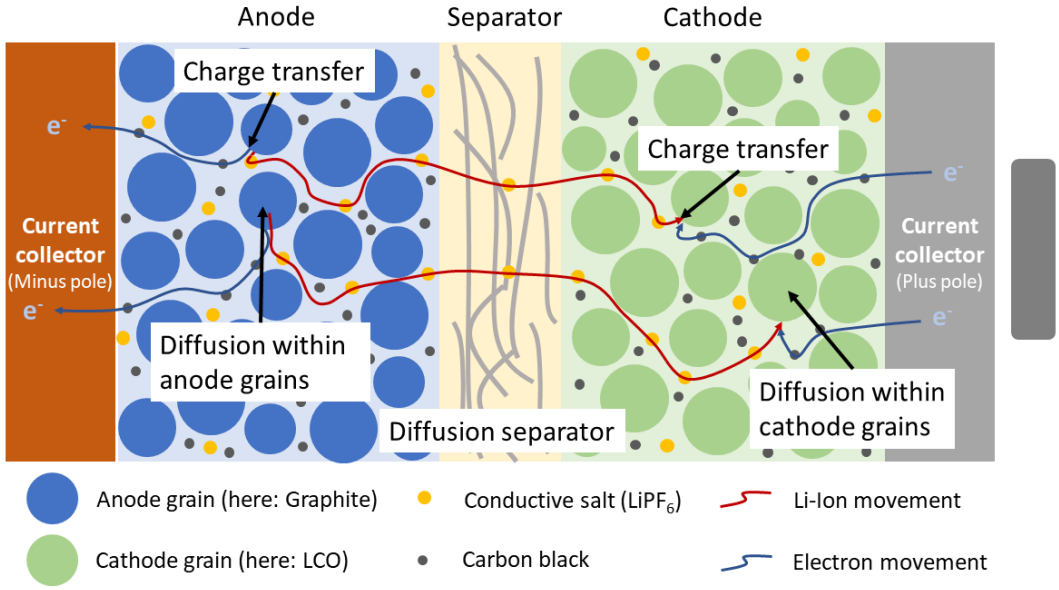

Figure 2.14 The movement of ions and electrons during discharge was examined using a lithium-ion battery with a lithium foil anode and a glassy carbon cathode as an example.

In order to generate an (approximately) correct chemical-physical equivalent circuit of the battery, the individual influence parameters of the chemical discharge process must be modeled in an equivalent circuit. Nevertheless, simplifications are still used here and, for example, the influence of the SEI layer on the surface of the anode is not taken into account. Figure 2.15 shows the equivalent circuit for the anode and the separator for a single reaction path.

A complete electrochemical model is usually too complex to be used to investigate actual processes in the battery. Therefore, a much-used approach is to simplify the model and to summarize or omit parameters that have only a minor influence on the equivalent circuit. A well-known simplification is the De Levie model, which completely neglects the effects of diffusion of ion and anion in separator, anode and cathode. In principle, the model can be further simplified. For example, it may be

possible to completely neglect the ohmic resistances in the anode and cathode. This results in a final equivalent circuit as shown in figure 2.15.

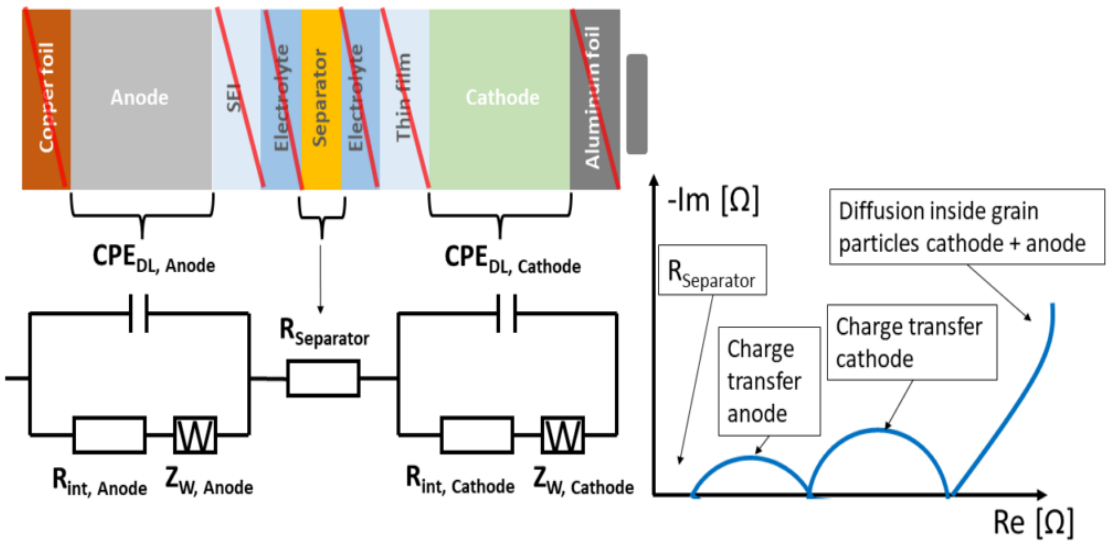

Figure 2.15 Simplified De Levie model of a complete cell. The admissibility of the simplification is not given as a general rule, but must be verified by suitable procedures.

However, the assessment of which parameters of the complete physical equivalent circuit can be neglected is not trivial. It must always be specifically checked in each individual case which simplifications are permissible without distorting the result. For example, if only high frequencies are investigated, ignoring diffusion in the separator, anode and cathode is perfectly justifiable, but for other investigations this adjustment may not be permissible. In other words, the De Levie model may have excellent accuracy in one case and completely fail for another cell in a different set of experiments.

2.4.4 X-ray absorption spectroscopy (XAS)

The inception of x-ray absorption spectroscopy (XAS) dates back over a century, and its progress has been substantial throughout the intervening years. However, because it grew out of a relatively unexplored area of scientific inquiry and was only studied by a small group of dedicated scholars, this methodology was at first seen as a fascinating curiosity that had no practical use and lacked a complete and strong

theoretical framework that could explain and predict experimental observations made on gaseous, liquid, and solid (both crystalline and amorphous) substances. Fourier analysis was used by Sayers, Stern, and Lytle in 1971 to flip the experimental data they got from photoelectron wave-vector space, turning it into a radial distribution function. The initial determination of quantitative values was conducted for bond distance, coordination number, temperature, and disorder features. The field has made significant advancements at an exponential rate over the course of 44 years following the publication of that fundamental work. X-ray absorption spectroscopy (XAS) and its associated methodologies are currently regarded as essential tools for advanced research in a wide range of disciplines, including materials science, solid-state physics and chemistry, catalysis, chemistry, biology, medicine, earth science, environmental studies, cultural heritage preservation, and nanoscience, among others. This introduction chapter provides a comprehensive summary of the key advancements that have contributed to the extensive utilization of XAS and its associated techniques for scientific characterization.

2.4.4.1 Principle of XAS

The core principles underlying X-ray absorption spectroscopy can be succinctly elucidated within a concise statement. When a sample is exposed to an X-ray photon of sufficient energy, it has the potential to ignite a core electron within the material. The energy levels of the core electrons remain largely unaltered by the chemical environment in which they reside due to their occupation of confined states. The selectivity of X-ray absorption spectroscopy (XAS) can be attributed to this particular component. The phrase "absorption edge" denotes the specific energy threshold at which a sudden and significant alteration occurs in the absorption coefficient. This particular aspect is indicative of the binding energy associated with the core level. The absorption edges, often referred to as sudden rises in absorption, correlate to the energy required for the ejection of a core electron into the lowest unoccupied molecular orbital (LUMO) or into the continuum, resulting in the creation of a photoelectron. The absorption discontinuity associated with the photoelectron originating from a 1s core level is commonly known as the K-edge. Conversely, the term "L-edge" is employed to denote the ionization event resulting from the excitation

or removal of a 2s or 2p electron. According to the data shown in Figure 2.16, the electron in an excited state possesses the capability to transition to either unoccupied bound levels or continuous unbound levels.

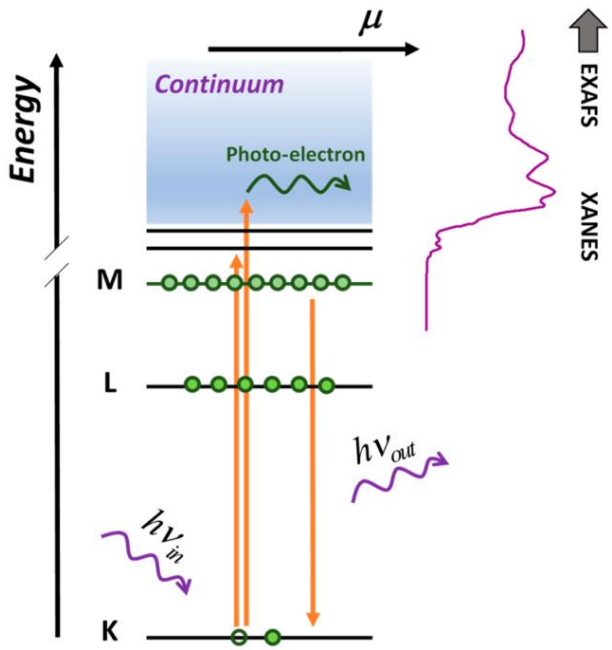

Figure 2.16 Scheme of the X-ray absorption process (Fracchia, Ghigna, Vertova, Rondinini, and Minguzzi, 2018).

The atoms in its vicinity can then scatter it back, a process known as back-diffusion. The interatomic distance determines whether the emitted electron and the back-scattered waves have a destructive or constructive interaction for a given photon energy. The result of this effect is a fluctuation in the X-ray absorption coefficient that can be measured hundreds of electron volts (eV) above the absorption edge. This allows one to determine the local structure (number, nature, and distance of surrounding atoms) in the area immediately surrounding the photo absorber; this is known as the "Extended X-ray Absorption Fine Structure" (EXAFS). Specifically, the absorption coefficient strongly modulates at energies near the boundary. In this case, the electronic transitions to bound unoccupied states and/or multiple scattering events are responsible for the X-ray absorption near edge structure (XANES). Significant data on the surrounding coordination environment can be gleaned from XANES (type

of coordination and its distortions). In conclusion, the oxidation state is reflected in the fine energy at which the absorption edge falls, which is directly proportional to the electron density on the photo absorber. Therefore, XAS provides a reliable, objective measure of atomic oxidation states in compounds.

- **X-ray absorption near edge structure (XANES)**

X-ray absorption near-edge structure (XANES) spectra reveal the oxidation state and coordination environment of metal atoms with great specificity (Figure 2.17a). In general, higher oxidation states have higher K-edge absorption edge energies. The position of the incrementing changes as a result of 1s core hole shielding effects on the effective number of positive charges (or, in a simplified view, the oxidation state). As an example, in a single-electron atom, the electron feels the full charge of the positive nucleus. On the other hand, in a highly charged atom, the outer electrons are repelled by the negatively charged electrons and attracted to the positively charged nucleus. It takes more energy to excite an electron from an orbital when the metal's oxidation state is higher because a higher oxidation state results in a more positively charged atom. When a negative charge is applied to a metal, however, the X-ray energy spectrum changes to a lower level.

Transitions from 1s to np, where np is the lowest occupied p orbital of the absorbing atom, are the primary contributors to the K-edge spectrum. This transition, with l = 1 (where l is the quantum number of the orbital momentum), is permitted by quantum mechanics and is typically strong. Pre-edge features resulting from 1s to (n-1) d transitions provide additional insight for transition metals with partially occupied d orbitals. These have a low intensity (l = 2, so they are formally forbidden or dipole-forbidden), but they are detectable because they occur at energies just below the main absorption edge. When the ligand environment is broken from octahedral symmetry, the intensity of the pre-edge peak rises (Yano and Yachandra, 2009).

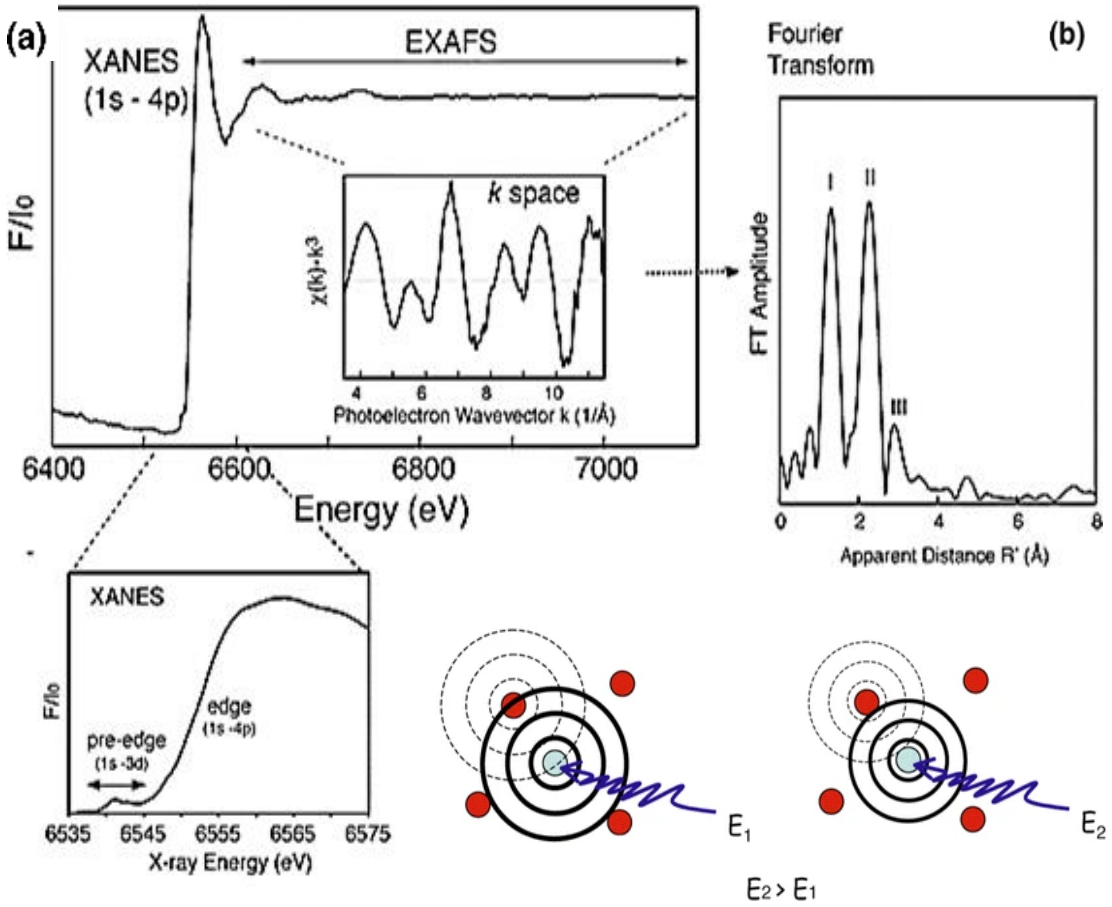

Figure 2.17 a) XANES and EXAFS spectra of the manganese K edge. Upper left: XANES and EXAFS regions of the X-ray absorption spectrum of a PS II sample, b) A diagram showing the propagating and reflected photoelectron wave, which represents interference in EXAFS (Yano and Yachandra, 2009).

- **Extended fine structure (EXAFS)**

Detailed information about the partial pair distribution functions of the atoms surrounding the absorber, such as distances, mean square deviations in distance, coordination numbers, and coordinating species, can be obtained through analysis of the extended x-ray absorption fine structure (EXAFS). EXAFS can be applied to any type of condensed matter, as its theory and interpretation do not rely on any assumptions of configurational symmetry or periodicity. EXAFS can be used on diluted systems because the fundamental physical process of x-ray absorption spectroscopy (XAS), the photo-excitation of a deep-core electron, is element specific. Thus, EXAFS

plays an important role in a wide range of scientific fields, including the study of life, the environment, chemistry, materials science, cultural heritage, and more. In a nutshell, EXAFS is a vital skill for any synchrotron radiation lab.

In XAS spectrum, the difference between XANES and EXAFS can be thought of as a difference in regime. One of the limitations of this definition is that there is no single, overarching principle that distinguishes the two systems in question, even though they appear to share the same conceptual principles. Most people place XANES at an energy level where the potential is 50 eV above the edge, while they place EXAFS at an energy level where the potential is between 50 and 1000 eV above the edge (Yano and Yachandra, 2009).

In the context of EXAFS (Extended X-ray Absorption Fine Structure), k-space and R-space are two crucial domains used for data analysis.

1. k-space: This is the energy domain used to analyze the variations in X-ray absorption due to the excited electrons ejected from an atom. In EXAFS, k represents the wave vector of the excited electrons, measured in Ångström^{-1} (Å^{-1}). Analyzing data in k-space involves studying the interference patterns of these outgoing and backscattered electron waves, which helps identify the scattering processes and energy changes.

2. R-space: This is the distance domain used to analyze the distribution of atoms around the central atom. In EXAFS, R represents the radial distance between the central atom and its neighboring atoms, measured in Ångström (Å). Data in R-space is obtained through Fourier transform of the k-space data, allowing determination of interatomic distances, coordination numbers, and the atomic distribution within the structure.

2.5 Thesis motivation

In this section, the research's origins will be addressed, drawing inspiration from two research studies. This has led to questions, challenges that arise, and problems that need to be solved based on the above research.

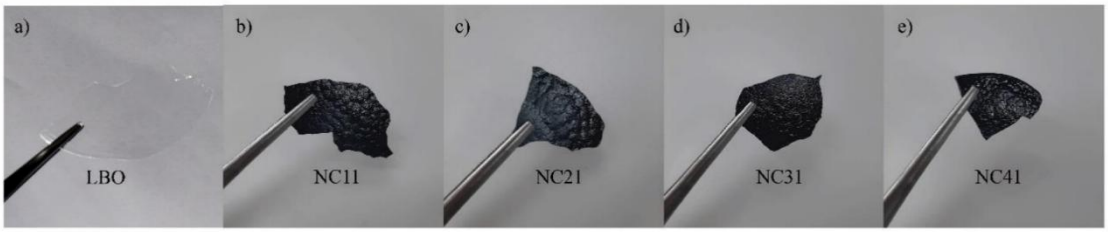

Figure 2.18 The plate glasses of a) LBO glass and b) - e) Ni/Co doped LBO, with the Ni:Co ratios being 1:1, 2:1, 3:1, and 4:1, respectively (Siriroj et al., 2023).

Due to the previous study titled "New glass cathode materials for Li-ion battery: Ni-Co doping in Li-B-O based glass" (Siriroj et al., 2023) which involved incorporating Ni-Co doping into LBO at a ratio of 0.2 (Ni-Co) to 0.8 LBO and varying the Ni and Co concentrations. Figure 2.18 shows the physiological characteristics of the glass plate sample. In electrochemical testing of glass cathodes, the glass cathode with a high cobalt (Co) content (NC11 which uses a Ni-CO ratio of 1:1) initially exhibited the highest specific capacity (380 mAh/g) during its first discharge cycle (Figure 2.19a).

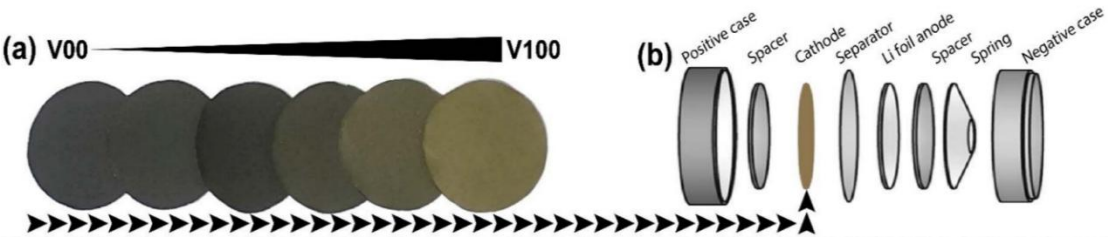

Figure 2.19 This figure show (a) The photograph of film composition of V_2O_5 from black color (0%) to yellowish-brown color (100%). (b) The coin cell assembly components (Siriroj et al., 2022).

However, in subsequent cycles, there was a significant decrease in capacity due to the entrapment of lithium ions in the glassy structure. Conversely, glass cathodes with a higher concentration of nickel ions in the co-doped Ni/Co-LBO glass (NC41 which uses a Ni-CO ratio of 4:1) displayed improved long-term retention properties (Figure 2.20a), indicating that a nickel-rich composition might facilitate the release of free lithium ions from the host glass structure (Siriroj et al., 2023).

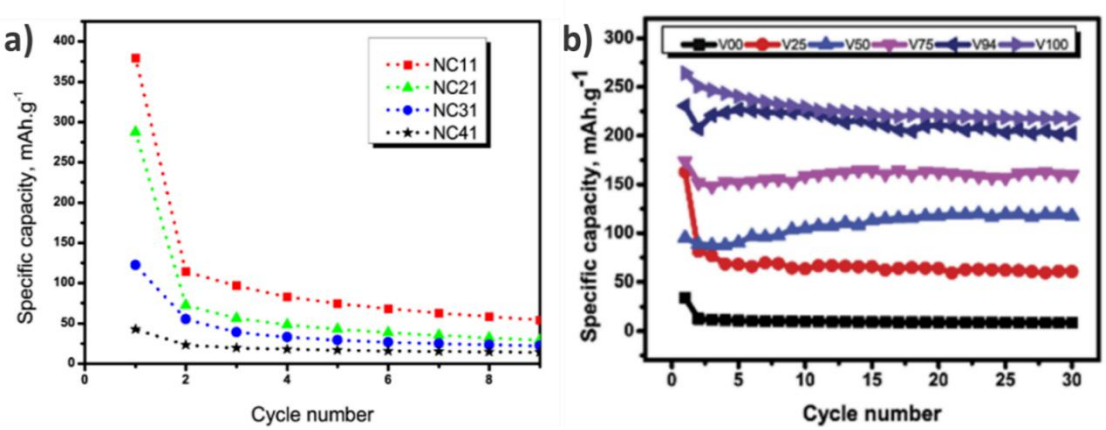

Figure 2.20 Shows specific capacitance value compared to test cycles of a) NC11, NC21, NC31 and NC41 (Siriroj et al., 2023). b) V00, V25, V50, V75, V94 and V100 (Siriroj et al., 2023; Siriroj et al., 2022).

For the reasons mentioned above, in the subsequent research on the topic "Enhancement of V_2O_5 Li-ion cathode stability by Ni/Co-doped Li-borate-based glass" the sample with the most stable capacitance value was selected. NC41 (25%) was incorporated into V_2O_5 (75%) and mixed for 24 hours, aiming to enhance the capacity to a higher level. Using symbols such as V00 to represent the absence of V_2O_5 (0%), and V100 to denote the presence of V_2O_5 at 100%. The cell was assembled using the coin cell technique. Figure 2.19a the cathode was constructed using a V_2O_5 mixed Ni/Co glass-based Li-borate film on an Al foil, featuring various compositional conditions, with a PP separator film (Celgard 2400) dividing it (Kayyar, Huang, Samiee, and Luo, 2012), while the anode consisted of Li foil. Afterward, it was infused with 50 microliters of 1 M $LiPF_6$ in an ethylene carbonate (EC): dimethyl carbonate (DMC) (1:1) electrolyte solution. Subsequently, the coin cell was sealed by utilizing an ECCCM-160E-A crimping

machine from MTI Corporation with a 1-ton push. In Figure 2.19b shows an overview of the components of a coin cell construction. The battery test results show that adding glass can change the voltage-capacity curve from pure V_2O_5 stairway form to a straighter line (Figure 2.20b).

Therefore, this work has piqued an interest in the glass-making process that is easy to make and produces the most efficient results through the traditional melt quenching method, drawing inspiration from two previous studies (Siriroj et al., 2023; Siriroj et al., 2022).

This study consisted of four distinct processes. In the initial process, Ni-Co and LBO were used, and this was followed by the glass melt quenching method, which was consistent with the methodology employed in a prior study (referenced as research (Siriroj et al., 2023)). The second process commenced by mixing the products of the first process with V_2O_5 before proceeding to the glass melt quenching method. In the third process, LBO, Ni, Co, and V_2O_5 were all combined and subjected to the glass melt quenching method simultaneously. The final process involved combining glass from the first process with V_2O_5 and mixing them for 24 hours to complete the procedure, mirroring the approach taken in another previous study (referred to as research (Siriroj et al., 2022)).

2.6 Sope and limitation

In this study, the scope and limitations revolve around materials, instrumentation, and research locations. Material selection is based on availability and alignment with research goals, while instrumentation is restricted by budget and technical constraints.

2.6.1 Materials

In this work, for the preparation of the glass base, we use Lithium carbonate (Li_2CO_3) with a purity of 99.5% and Boric acid (H_3BO_3) with a purity of 99.8%. Additionally, in the chemical doping part of this project, we employ other chemicals sourced from Himedia, including Nickel oxide (NiO) with a purity of 97.0%, Vanadium(V) oxide (V_2O_5) with a purity of 99.6%, and Coalt (II, III) oxide (Co_3O_4) with a purity of 70.0%.

2.6.2 Instrumentation and Research locations

In this research project, we operated under the guidance and assistance of the Battery and Energy Material Research Laboratory (Glass Novel Battery), which is a part of the Synchrotron Light Research Institute (a public organization). This study also involves the examination of sample materials using X-ray diffraction (XRD) techniques, overseen by the Science and Technology Instrumentation Center at Suranaree University of Technology.